Available online at www.sciencedirect.com

ScienceDirect

Nuclear Physics B 971 (2021) 115520

NUCLEAR PHYSICS B

www.elsevier.com/locate/nuclphysb

Model-independent study on the anomalous $\tau\bar{\tau}\gamma$ couplings at the ILC

M. Köksal

Department of Optical Engineering, Cumhuriyet University, 58140, Sivas, Turkey

Received 5 April 2021; received in revised form 5 August 2021; accepted 19 August 2021
Available online 24 August 2021
Editor: Hong-Jian He

Abstract

The potential of the process $\gamma\gamma \to \tau\bar{\tau}\gamma$ is examined in a model-independent way using the effective Lagrangian approach for the International Linear Collider, a proposed electron-positron machine which is designed with standard configurations of 0.25 TeV/2000 fb^{-1}, 0.35 TeV/200 fb^{-1} and 0.5 TeV/4000 fb^{-1}. The limits obtained for the tau lepton's anomalous magnetic dipole moment $\tilde{a}_\tau$ and the tau lepton's anomalous electric dipole moment $\tilde{d}_\tau$ defining the anomalous $\tau\bar{\tau}\gamma$ couplings at 95% confidence level and systematic uncertainties of $\delta_{sys} = 0, 5, 10\%$ are compared with the experimental results. The best limits obtained with $\delta_{sys} = 0\%$ on the anomalous couplings are $-0.00082 < \tilde{a}_\tau < 0.00050$ and $|\tilde{d}_\tau| < 3.59 \times 10^{-18}$ e cm, respectively. Also, the limits on the anomalous couplings do not improve proportionately to the luminosity due to the systematic error considered here. The reason of this situation is the systematic error which is much bigger than the statistical error. If the systematic error is improved, we expect better limits on the couplings. However, the best limits on the anomalous couplings for the process $\gamma\gamma \to \tau\bar{\tau}\gamma$ with $\sqrt{s} = 500$ GeV, $L_{int} = 4000$ fb^{-1} and $\delta_{sys} = 0\%$ can be improved up to 4 times for $\tilde{a}_\tau$ and 9 times for $\tilde{d}_\tau$ according to case with $\delta_{sys} = 10\%$. Our results show that $\gamma\gamma$ collisions at the ILC give results up to one order of magnitude for $\tilde{a}_\tau$ and two orders of magnitude for $\tilde{d}_\tau$ better than the current experimental limits.

E-mail address: mkoksal@cumhuriyet.edu.tr.

https://doi.org/10.1016/j.nuclphysb.2021.115520

1. Introduction

The magnetic moments of leptons have spurred the development of Quantum Field Theory and provided the most precise comparison between theory and experiment in the history of science. The magnetic dipole moment of the electron which is responsible for the interaction with the magnetic field in the Born approximation is given as follows

$$\vec{\mu} = g\frac{\mu_B}{\hbar}\vec{s} \tag{1}$$

where g is the Lande g-factor, μ_B is the Bohr magneton and $\vec{s}$ is the spin of the electron. For the electron, the value of g in the Dirac equation is 2. It is traditional to point out the deviation of g from 2 in terms of the value of the so-called anomalous magnetic moment. The anomalous magnetic moment of the electron is a dimensionless quantity and is described by $a_e = \frac{g-2}{2}$. The measured anomalous magnetic moment of the electron agrees with the Standard Model (SM) prediction to better than one part per billion [1].

However, recently, the Muon $g-2$ Experiment at Fermilab reported a measurement reading $a_\mu^{\text{FNAL}} = 116592040(54) \times 10^{-11}$, which is larger than the SM prediction $a_\mu^{\text{SM}} = 116591810(43) \times 10^{-11}$ in which contributions from QED, QCD and electroweak interactions are taken into account with highest precision [2,3]. This leads to $a_\mu^{\text{FNAL}} - a_\mu^{SM} = (230 \pm 69) \times 10^{-11}$, which corresponds to a 3.2σ discrepancy. Because the Fermilab observation is compatible with the long-standing discrepancy from the E821 experiment at BNL the overall deviation from the SM central value

$$\Delta a_\mu^{exp} = a\mu^{\text{FNAL+BNL}} - a_\mu^{\text{SM}} = (251 \pm 69) \times 10^{-11} \tag{2}$$

strengthens the significance to 4.2σ [2,4,5]. Even though the discrepancy is not statistically significant yet, it is interesting to entertain the possibility that it corresponds to a real signal of new physics. Besides, new physics beyond the SM is anticipated to modify the SM prediction of the anomalous magnetic moment of a lepton ℓ of m_ℓ mass by a contribution of order $\sim m_\ell^2/\Lambda^2$ [6]. Thus, given the large factor $(m_\tau/m_\mu)^2 \cong 283$, the anomalous magnetic moment of the tau lepton is much more sensitive than the one of the muon to the electroweak and new physics effects which give contribution $\sim m_\ell^2$, making its measurement an excellent opportunity to unveil or constrain new physics effects.

New physics beyond the SM presents the theoretical developments needed to enlighten the problems of the SM, such as the strong CP problem, neutrino oscillations, matter−antimatter asymmetry in the universe. One of the ways to research new physics beyond the SM is the effective Lagrangian method [7]. The effective Lagrangian method is based upon the assumption that at higher energy regions beyond the SM, there is a more fundamental physics that reduces to the SM at lower energy regions. In this method, one adds higher dimensional effective operators suppressed by an energy cut-off (Λ) with the SM fields and obtain the interactions after symmetry breaking. A subset of these effective operators can modify the SM $\tau\tau\gamma$ interactions through the effective Lagrangian method can be examined.

In this work, we study the effects of the anomalous $\tau\bar{\tau}\gamma$ couplings defined with the effective Lagrangian method in the model-independent approach between the tau lepton and the photon for the process $\gamma\gamma \to \tau\bar{\tau}\gamma$ at the International Linear Collider (ILC). The most general anomalous vertex function determining $\tau\bar{\tau}\gamma$ interaction between two on-shell tau leptons and a photon is given by [8,9]

$$\Gamma^{\nu} = F_1(q^2)\gamma^{\nu} + \frac{i}{2m_\tau}F_2(q^2)\sigma^{\nu\mu}q_\mu + \frac{1}{2m_\tau}F_3(q^2)\sigma^{\nu\mu}\gamma^5 q_\mu. \tag{3}$$

Here, $\sigma^{\nu\mu} = \frac{i}{2}(\gamma^{\nu}\gamma^{\mu} - \gamma^{\mu}\gamma^{\nu})$, q represents the momentum transfer to the photon and $m_\tau = 1.777$ GeV shows the tau lepton's mass. $F_1(q^2)$ and $F_2(q^2)$ are the Dirac and Pauli form factors, $F_3(q^2)$ is the electric dipole form factor. The last term $\sigma^{\nu\mu}\gamma^5$ breaks the CP symmetry, so the coefficient $F_3(q^2)$ determines the strength of a possible CP violation process, which might originate from new physics. $F_1(q^2)$, $F_2(q^2)$ and $F_3(q^2)$ form factors in limit $q^2 \to 0$ are equal to the formulas below

$$F_1(0) = 1,\ F_2(0) = a_\tau,\ F_3(0) = \frac{2m_\tau d_\tau}{e}, \tag{4}$$

where a_τ is the magnetic dipole moment of the tau lepton and d_τ is the electric dipole moment of the tau lepton.

In a lot of works examining the anomalous magnetic and electric dipole moments of the tau lepton, the tau leptons or the photon in $\tau\bar{\tau}\gamma$ couplings are off-shell [10–14]. In this case, since the tau lepton is off-shell, the couplings analyzed in those works are not the anomalous a_τ and d_τ. Hence, we will name the anomalous magnetic and electric dipole moments of the tau lepton examined as $\tilde{a}_\tau$ and $\tilde{d}_\tau$ instead of a_τ and d_τ. Thus, the possible deviation from the SM predictions of $\tau\bar{\tau}\gamma$ couplings could be examined in the effective Lagrangian method. In this method, the anomalous $\tau\bar{\tau}\gamma$ couplings are parameterized using high dimensional effective operators. In this work, we consider the dimension-six operators that contribute to the magnetic and electric dipole moments of the tau lepton. These operators are presented as follows [15]

$$Q_{LW}^{33} = (\bar{\ell_\tau}\sigma^{\mu\nu}\tau_R)\sigma^I\varphi W^I_{\mu\nu}, \tag{5}$$

$$Q_{LB}^{33} = (\bar{\ell_\tau}\sigma^{\mu\nu}\tau_R)\varphi B_{\mu\nu}. \tag{6}$$

Here, φ and ℓ_τ represent the Higgs and the left-handed $SU(2)$ doublets, σ^I show the Pauli matrices and $W^I_{\mu\nu}$ and $B_{\mu\nu}$ are the gauge field strength tensors. Thus, the effective Lagrangian can be written as follows

$$L_{eff} = \frac{1}{\Lambda^2}[C_{LW}^{33}Q_{LW}^{33} + C_{LB}^{33}Q_{LB}^{33} + h.c.]. \tag{7}$$

After electroweak symmetry breaking, contributions to the magnetic and electric dipole moments of the tau lepton are given by

$$\kappa = \frac{2m_\tau}{e}\frac{\sqrt{2}\upsilon}{\Lambda^2}Re[\cos\theta_W C_{LB}^{33} - \sin\theta_W C_{LW}^{33}], \tag{8}$$

$$\tilde{\kappa} = -\frac{\sqrt{2}\upsilon}{\Lambda^2}Im[\cos\theta_W C_{LB}^{33} - \sin\theta_W C_{LW}^{33}]. \tag{9}$$

Here, υ represents the vacuum expectation value and $\sin\theta_W$ shows the weak mixing angle. The relations between κ and $\tilde{\kappa}$ parameters with $\tilde{a}_\tau$ and $\tilde{d}_\tau$ are defined by

$$\kappa = \tilde{a}_\tau, \quad \tilde{\kappa} = \frac{2m_\tau}{e}\tilde{d}_\tau. \tag{10}$$

The electron and muon anomalous magnetic moments can be studied with high sensitivity via spin precession experiments. On the other hand, since the tau lepton has a much shorter lifetime than other leptons it is extremely difficult to measure the magnetic moment of the tau lepton by using spin precession experiments. Instead of spin precession experiments, the magnetic moment measurement of the tau lepton is carried out at collider experiments.

Experimental limits at 95% confidence level on the magnetic moment of the tau lepton were derived the processes $e^-e^+ \to \tau^-\tau^+\gamma$ and $e^-e^+ \to e^-\gamma^*\gamma^*e^+ \to e^-\tau^-\tau^+e^+$ by L3, OPAL and DELPHI Collaborations by the Large Electron Positron Collider (LEP) [16–18]

$$\text{L3} : -0.052 < \tilde{a}_\tau < 0.058, \tag{11}$$

$$\text{OPAL} : -0.068 < \tilde{a}_\tau < 0.065, \tag{12}$$

$$\text{DELPHI} : -0.052 < \tilde{a}_\tau < 0.013. \tag{13}$$

CP violation was originally discovered in neutral K mesons [19]. This phenomenon has been described within the SM by the complex couplings in the Cabibbo-Kobayashi-Maskawa (CKM) matrix of the quark sector [20]. Actually, there is no CP violation in the leptonic couplings in the SM. In spite of that, CP violation in the quark sector induces electric dipole moment of the leptons in the three loop level. This contribution of the SM to the electric dipole moment of the leptons can be shown to be too small to detect [21]. If there considers a coupling of leptons in new physics beyond the SM, electric dipole moment may induce the detectable size of CP-violation [22–29].

The experimental results on the $\tilde{d}_\tau$ coupling at 95% confidence level at the LEP are [16–18,30]

$$\text{L3} : |\tilde{d}_\tau| < 3.1 \times 10^{-16}\, e\,\text{cm}, \tag{14}$$

$$\text{OPAL} : |\tilde{d}_\tau| < 3.7 \times 10^{-16}\, e\,\text{cm}, \tag{15}$$

$$\text{DELPHI} : |\tilde{d}_\tau| < 3.7 \times 10^{-16}\, e\,\text{cm}, \tag{16}$$

$$\text{BELLE} : -2.2 < Re(\tilde{d}_\tau) < 4.5 \times (10^{-17}\, e\,\text{cm}), \tag{17}$$

$$\text{BELLE} : -2.5 < Im(\tilde{d}_\tau) < 0.8 \times (10^{-17}\, e\,\text{cm}). \tag{18}$$

As a result, the magnetic and electric dipole moments of the tau lepton allow stringent testing for new physics beyond SM and have been studied in detail by Refs. [31–49].

The advantage of linear colliders with respect to hadron colliders is in the general cleanliness of the events where two elementary particles, electron and positron beams, collide at high energy, and the high resolutions of the detector are made possible by the relatively low absolute rate of background events. One of the most realistic linear colliders is the ILC. Since the ILC has a much cleaner environment than the LHC, it may be able to observe the smallest deviation from the SM estimates that point to new physics, discover new particles and make precise measurements of them. The ILC is planned to run at center-of-mass energies of 250, 350 and 500 GeV, with total integrated luminosities of 2000, 200 and 4000 fb^{-1}, respectively [50]. An increase of up to 1 TeV is also considered for center-of-mass energy, which we do not include in our calculations [51].

2. Cross sections and sensitivity analysis

The expected design of the future linear colliders will include operation also in $e\gamma$ and $\gamma\gamma$ modes. In $e\gamma$ and $\gamma\gamma$ processes, real photon beams can be generated by converting the incoming e^- and e^+ beams into photon beams through the Compton backscattering mechanism. The maximum collision energy is expected to be 80% for $\gamma\gamma$ collision and 90% for $e\gamma$ collision of the original e^-e^+ collision energy. However, the expected luminosities are 15% for $\gamma\gamma$ collision and 39% for $e\gamma$ collision of e^-e^+ luminosities [52]. On the other hand, when using directly the lepton beams, quasi-real photons will be radiated at the interaction allowing

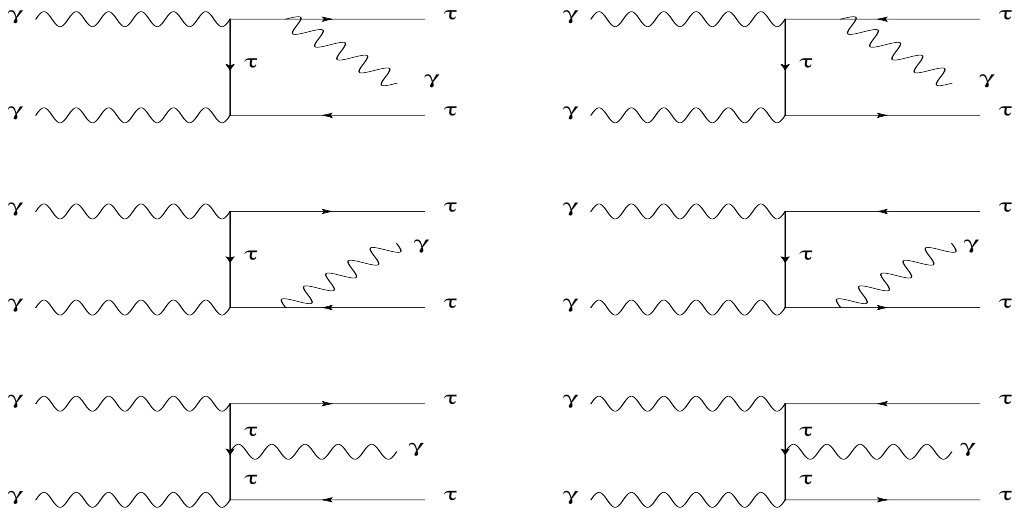

Fig. 1. Tree-level Feynman diagrams for the process $\gamma\gamma \to \tau\bar{\tau}\gamma$.

for processes like $e\gamma^*$ and $\gamma^*\gamma^*$ that occur by emission from the electron/positron beam using the Equivalent Photon Approximation [53,54]. DELPHI Collaboration based on the process $e^-e^+ \to e^-\gamma^*\gamma^*e^+ \to e^-\tau^-\tau^+e^+$ through the subprocess $\gamma^*\gamma^* \to \tau^-\tau^+$ have obtained the limits on the electromagnetic moments. Here, γ^* photons from the incoming e^- and e^+ beams scatter at very small angles from the beam pipe. Therefore, these photons have very low virtuality and we say that these photons are almost-real. As known, the center-of-mass energy of $\gamma\gamma$ collisions is much greater than that of $\gamma^*\gamma^*$ collisions. This gives us an important advantage in the search for new physics beyond the SM.

Secondly, the process $\gamma\gamma \to \tau\tau$ has a larger cross section than the process $\gamma\gamma \to \tau\tau\gamma$ that is on the mass shell of the photon in the final state. On the other hand, decay products of the tau leptons are highly collimated because of the QCD jets and this makes them difficult to identify. However, the final state photon identification can facilitate the tau pair identification. Generally, the anomalous parameters tend to increase the cross section for the process $\gamma\gamma \to \tau\tau\gamma$, especially for photons with high energy which are well isolated from the decay products of the taus [55]. Furthermore, the single-photon in the final state has the advantage of being identified with high efficiency and purity.

The effects of anomalous contributions arising from dimension-six operators and SM contributions as well as interference between new physics and the SM contribution is performed through the process $\gamma\gamma \to \tau\bar{\tau}\gamma$ at the ILC. For this purpose, in Fig. 1, Feynman diagrams of the process $\gamma\gamma \to \tau\tau\gamma$ that is on the mass shell of the photon in the final state are represented. As seen in Fig. 1, the total number of diagrams is 6. Here, the contribution to new physics comes from all diagrams that consist of t and u channels. Also, the arrows represented in this diagram are momentum arrows. On the other hand, we do not take into account initial state radiation in this study.

Incoming photons in the process $\gamma\gamma \to \tau\bar{\tau}\gamma$ are Compton backscattered photons. The spectrum of Compton backscattered photons is given as follows [56]

$$f_{\gamma/e}(y) = \frac{1}{g(\zeta)}\left[1 - y + \frac{1}{1-y} - \frac{4y}{\zeta(1-y)} + \frac{4y^2}{\zeta^2(1-y)^2}\right] \tag{19}$$

where

$$g(\zeta) = \left(1 - \frac{4}{\zeta} - \frac{8}{\zeta^2}\right) log(\zeta + 1) + \frac{1}{2} + \frac{8}{\zeta} - \frac{1}{2(\zeta + 1)^2} \tag{20}$$

with

$$y = \frac{E_\gamma}{E_e},\ \zeta = \frac{4E_0E_e}{M_e^2},\ y_{max} = \frac{\zeta}{1+\zeta} \tag{21}$$

where E_γ represents the energy of the backscattered, E_0 and E_e show energy of the incoming laser photon and initial energy of the electron beam before Compton backscattering. Also, the maximum value of y reaches 0.83 when $\zeta = 4.8$.

The total cross section of the process $\gamma\gamma \to \tau\bar{\tau}\gamma$ can be given by the following integration [57]:

$$d\sigma(e^-e^+ \to \gamma\gamma \to \tau\bar{\tau}\gamma) = \int_{z_{min}}^{z_{max}} dz\, 2z\, d\hat{\sigma}(\gamma\gamma \to \tau\bar{\tau}\gamma) \times \int_{z^2/y_{max}}^{y_{max}} \frac{dy}{y} f_{\gamma/e}(y) f_{\gamma/e}(z^2/y). \tag{22}$$

Here, $d\hat{\sigma}(\gamma\gamma \to \tau\bar{\tau}\gamma)$ represents the cross section of the process and the center-of-mass energy of e^-e^+ system, $\sqrt{s}$, is related to the center-of-mass energy of $\gamma\gamma$ system, $\sqrt{\hat{s}}$ by $\hat{s} = z^2 s$. As can be seen from Fig. 1, since the process $\gamma\gamma \to \tau\bar{\tau}\gamma$ includes three anomalous vertices, thus the total cross sections are written up to the 6th power of the anomalous couplings. The total cross section of process $\gamma\gamma \to \tau\bar{\tau}\gamma$ is an even function of $\tilde{\kappa}$ and a nonzero value of this parameter always has a constructive effect on the total cross section. Thus, contributions to the total cross section of $\tilde{\kappa}$ are proportional to $\tilde{\kappa}^2$ or higher order even power:

$$\sigma(\tilde{\kappa}) = \sigma^3\tilde{\kappa}^6 + \sigma^2\tilde{\kappa}^4 + \sigma^1\tilde{\kappa}^2 + \sigma_{SM}. \tag{23}$$

Besides, the effect of κ parameter on the total cross section is given by:

$$\sigma(\tilde{\kappa}) = \sigma^9\kappa^6 + \sigma^8\kappa^5 + \sigma^7\kappa^4 + \sigma^6\kappa^3 + \sigma^5\kappa^2 + \sigma^4\kappa + \sigma_{SM}. \tag{24}$$

Here, σ_{SM} is the contribution of the SM, $\sigma^i (i = 1 - 9)$ are the anomalous contribution. Also, σ^9 and σ^3 coefficients are same [58]. It can be seen that the total cross sections of the process $\gamma\gamma \to \tau\bar{\tau}\gamma$ are symmetric for the anomalous $\tilde{\kappa}$ coupling, it is nonsymmetric for κ. Thus, we anticipate that while the limits on the anomalous magnetic dipole moment are asymmetric, the limits on the electric dipole moment are symmetric.

The tau lepton is the heaviest charged lepton that decays into lighter leptons, electron, muon and lighter hadrons such as π and K. Primary decay channels are given with one prong decay

$$\tau \to \nu_\tau + \ell + \bar{\nu_\ell},\ \ell = e, \mu, \tag{25}$$

$$\tau \to \nu_\tau + \pi^\pm, \tag{26}$$

$$\tau \to \nu_\tau + \pi^\pm + \pi^0, \tag{27}$$

$$\tau \to \nu_\tau + \pi^\pm + \pi^0 + \pi^0. \tag{28}$$

Also, three prong decays are given as follows

$$\tau \to \nu_\tau + 3\pi^\pm + n\pi^0. \tag{29}$$

Produced particles from tau decays are called tau jets due to the fact that the number of daughter particles is always greater than one. One prong lepton jets are detected by similar algorithms used by direct electron and muon. Identification of hadronic jets is more complicated than leptonic modes because of the QCD jets as background. Nevertheless, tau jets are highly collimated. On the other hand, tau identification efficiency depends of a specific process, background processes, some kinematic parameters and luminosity. Investigations of tau identification have not been examined yet for the ILC detectors. In this case, identification efficiency can be parameterized as a function of transverse momentum and rapidity of the tau lepton [59]. The following cuts for the selection of the tau leptons can be applied as used in many studies: $p_T^\tau = p_T^{\bar\tau} > 20$ GeV, $|\eta^\tau| = |\eta^{\bar\tau}| < 2.5$ [38]; $p_T^\tau = p_T^{\bar\tau} > 10$ GeV, $|\eta^\tau| = |\eta^{\bar\tau}| < 2.5$ [60]. These cuts on the tau leptons ensure that their decay products are collimated which allows their momenta to be reconstructed reasonably accurately, despite the unmeasured energy going into neutrinos [60]. Therefore, in this study, we consider the transverse momentums and rapidities of the taus as $p_T^\tau = p_T^{\bar\tau} > 15$ GeV, $|\eta^\tau| = |\eta^{\bar\tau}| < 2.5$.

We know that the high dimensional operators could affect p_T distribution of the photon, especially at the region with a large p_T values, which can be very useful to distinguish signal and background events. For this purpose, we use the following cuts set: p_T^τ, $p_T^{\bar\tau}$, p_T^γ, $|\eta^\tau|$, $|\eta^{\bar\tau}|$, $|\eta^\gamma|$, $\Delta R(\tau,\bar\tau)$, $\Delta R(\tau,\gamma)$, $\Delta R(\bar\tau,\gamma)$ where p_T is the transverse momentum of each particle in the final state, $|\eta|$ is the pseudorapidity of each particle in the final state and $\Delta R = \sqrt{\Delta\phi^2 + \Delta\eta^2}$ is Euclidean distance in coordinates of pseudorapidity and azimuthal angle. We apply $p_T^\tau = p_T^{\bar\tau} > 15$ GeV, $p_T^\gamma > 10$ GeV, $|\eta^\tau| = |\eta^{\bar\tau}| = |\eta^\gamma| < 2.5$ and $\Delta R(\tau,\bar\tau) = \Delta R(\tau,\gamma) = \Delta R(\bar\tau,\gamma) > 0.4$ with tagged Cut-1, four different values of p_T^γ with tagged Cut-2, Cut-3, Cut-4, and Cut-5 changing according to center-of-mass energies. In this study, the processes $e^-e^+ \to Z/\gamma^* \to \tau\tau\gamma$ and $e^-e^+ \to e^-\gamma^*\gamma^* e^+ \to e^-\tau\tau\gamma e^+$, which give the same final state as our process, can be considered as background. At the highest center-of-mass energy, while the value of the cross section of the process $e^-e^+ \to Z/\gamma^* \to \tau\tau\gamma$ using cut set in Cut-1 is 0.104 pb, the cross section of the process $e^-e^+ \to e^-\gamma^*\gamma^* e^+ \to e^-\tau\tau\gamma e^+$ is obtained as 0.0053 pb. The total cross sections of these backgrounds are quite small with respect to the SM cross section of the process $\gamma\gamma \to \tau\tau\gamma$ (σ_{SM} =0.535 pb). However, we examine the transverse momentum distributions of the photon in the final state for the signal and possible backgrounds at the center-of-mass energy of 0.5 TeV. Figs. 2 and 3 show p_T^γ photon transverse momentum distributions of the process $\gamma\gamma \to \tau\tau\gamma$ signal and backgrounds with $\kappa = 0.005$ and $\tilde\kappa = 0.005$ at the center-of-mass energy of 0.5 TeV, respectively. In these figures, the solid histogram corresponds to signal of the process $\gamma\gamma \to \tau\tau\gamma$, and the dashed distributions correspond to the other SM backgrounds. As can be seen from the figures, the SM prediction of the process $\gamma\gamma \to \tau\tau\gamma$ is much larger than the other background contributions. For this reason, we only take into account the SM cross section of the process $\gamma\gamma \to \tau\tau\gamma$ in this study as a background.

A summary of the cuts is shown in Table 1. For three center-of-mass energies, the total cross sections of the process $\gamma\gamma \to \tau\bar\tau\gamma$ as a function of the anomalous κ and $\tilde\kappa$ couplings for kinematic cuts described in Table 1 are given in Figs. 4–9. As can be seen from these figures, the changes of the total and the SM cross sections according to κ and $\tilde\kappa$ couplings have similar characteristics. In addition, after each kinematic cut is applied, the cross sections decrease as expected. To take a closer look at these rates of change, Table 2 has been presented. In Table 2, we give the total cross sections and the SM cross section of the process $\gamma\gamma \to \tau\bar\tau\gamma$ with respect

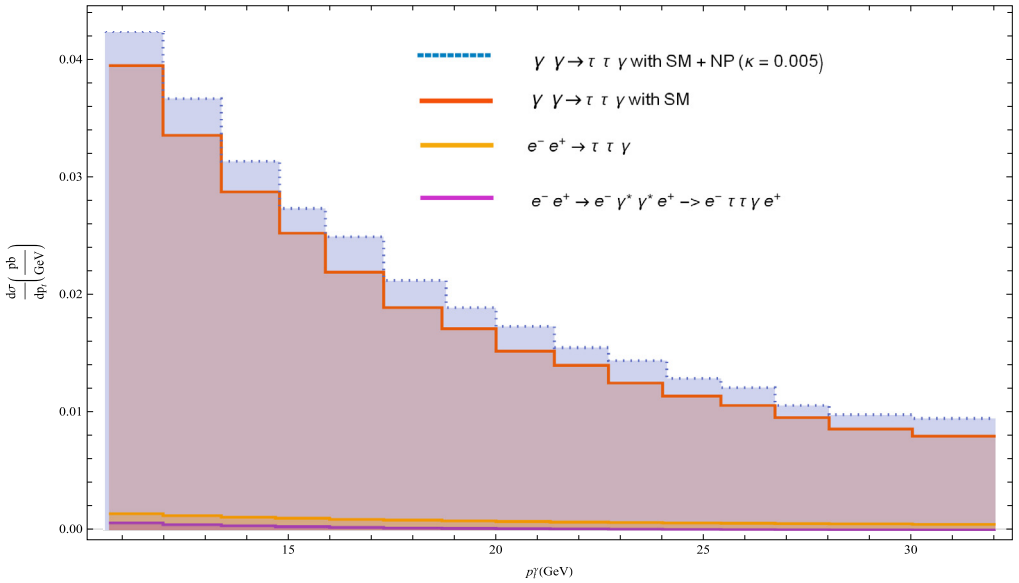

Fig. 2. p_T^{γ} photon transverse momentum distributions of the process $\gamma\gamma \to \tau\tau\gamma$ signal and backgrounds with $\kappa = 0.005$ at $\sqrt{s}$ =0.5 TeV. (For interpretation of the colors in the figure(s), the reader is referred to the web version of this article.)

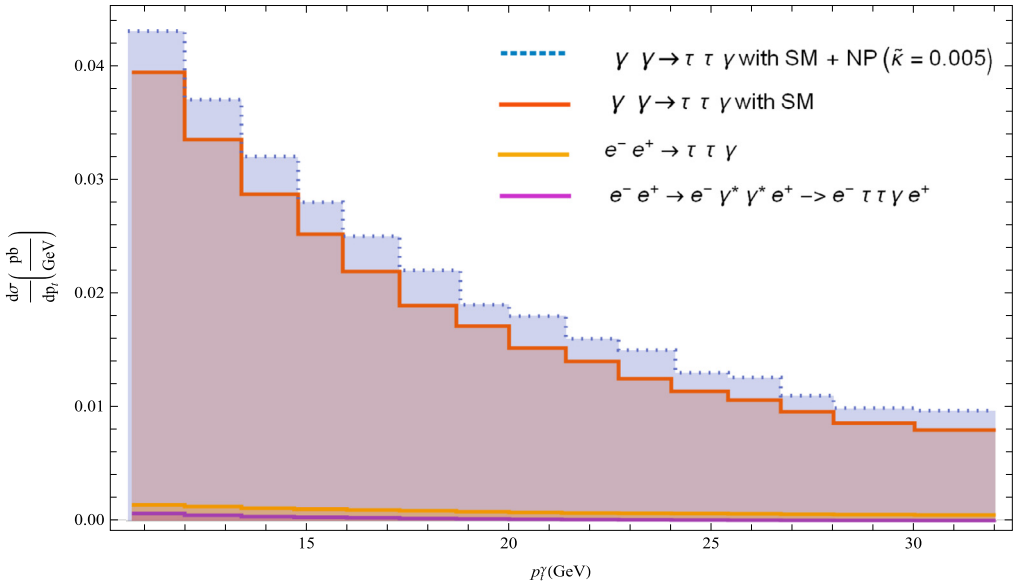

Fig. 3. Same as in Fig. 2, but for $\tilde{\kappa} = 0.005$.

to different kinematic cuts. As can be understood from Table 2, the ratios arise from the total cross sections divided by the SM cross sections and increase after each applied kinematic cut. As the applied kinematic cuts increase, the SM cross section is suppressed, thus the signal becomes more apparent. Thus, we observe the total and SM cross sections of the process $\gamma\gamma \to \tau\bar{\tau}\gamma$ with Cut-5 of each center-of-mass energy.

Table 1
Descriptions of kinematic cuts used for analysis.

Cuts	Definitions
Cut-1	$p_T^{\tau} = p_T^{\bar{\tau}} > 15$ GeV $+ p_T^{\gamma} > 10$ GeV $+$ $\lvert\eta^{\tau}\rvert = \lvert\eta^{\bar{\tau}}\rvert = \lvert\eta^{\gamma}\rvert < 2.5 + \Delta R(\tau, \bar{\tau}) =$ $\Delta R(\tau, \gamma) = \Delta R(\bar{\tau}, \gamma) > 0.4$
Cut-2	Same as in Cut-1, but for $p_T^{\gamma} > 15$ GeV
Cut-3	Same as in Cut-1, but for $p_T^{\gamma} > 20$ GeV
Cut-4	Same as in Cut-1, but for $p_T^{\gamma} > 25$ GeV
Cut-5	Same as in Cut-1, but for $p_T^{\gamma} > 30$ GeV

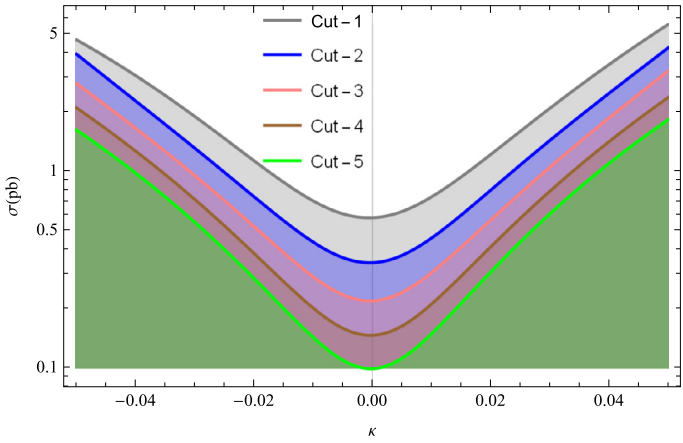

Fig. 4. The total cross sections of the process $\gamma\gamma \to \tau\bar{\tau}\gamma$ with $\sqrt{s} = 250$ GeV beam as a function of the anomalous κ couplings at five different kinematic cuts.

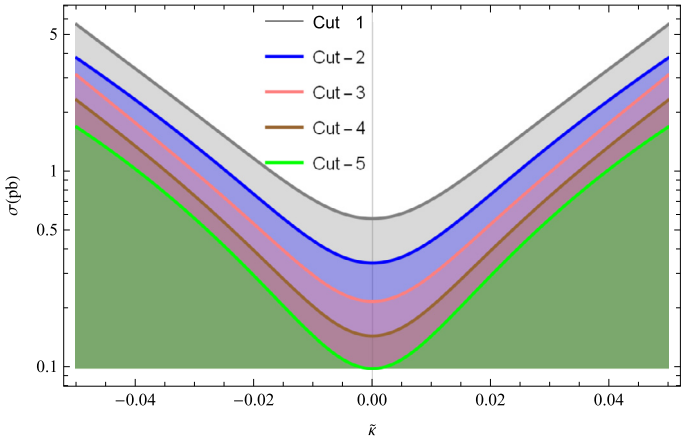

Fig. 5. Same as in Fig. 4, but for the anomalous $\tilde{\kappa}$ couplings.

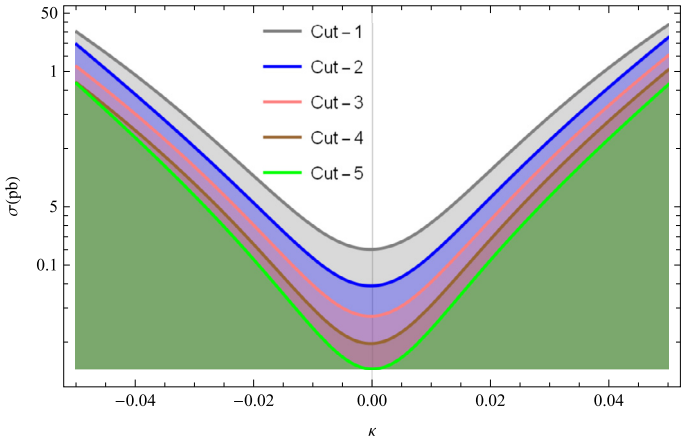

Fig. 6. The total cross sections of the process $\gamma\gamma \to \tau\bar{\tau}\gamma$ with $\sqrt{s} = 350$ GeV beam as a function of the anomalous κ couplings at five different kinematic cuts.

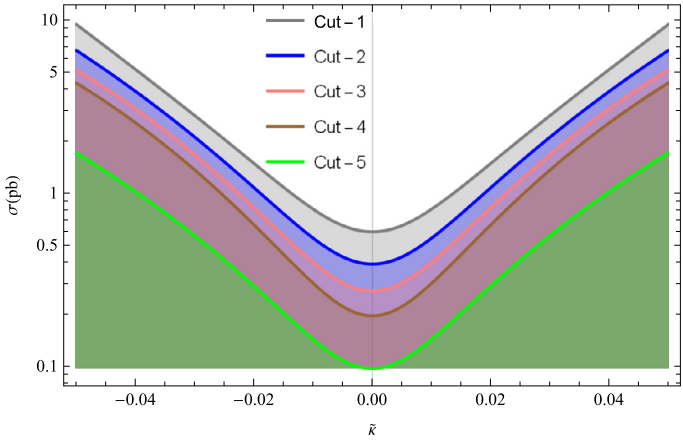

Fig. 7. Same as in Fig. 6, but for the anomalous $\tilde{\kappa}$ couplings.

Figs. 10 and 11 present the results for the total cross sections of the process $\gamma\gamma \to \tau\bar{\tau}\gamma$ at $\sqrt{s} = 250, 350, 500$ GeV depending on κ and $\tilde{\kappa}$ parameters. Here, we assume that only one of two anomalous couplings deviate from the SM at any given time. The total cross sections show a clear dependence according to the center-of-mass energy and the anomalous couplings. As can be seen from these figures, the deviation from the SM of the total cross sections including the anomalous couplings at $\sqrt{s} = 500$ GeV is larger than the other center-of-mass energies. Thus, we expect that the obtained limits on the anomalous κ and $\tilde{\kappa}$ couplings at $\sqrt{s} = 500$ GeV are to be more restrictive than the limits at $\sqrt{s} = 250, 350$ GeV. Moreover, the effects of the anomalous κ and $\tilde{\kappa}$ couplings on the total cross sections of the process $\gamma\gamma \to \tau\bar{\tau}\gamma$ are shown in Figs. 12–14.

We use χ^2 analysis with systematic errors to study the sensitivities on the anomalous $\tilde{a}_\tau$ and $\tilde{d}_\tau$ dipole moments of the τ lepton:

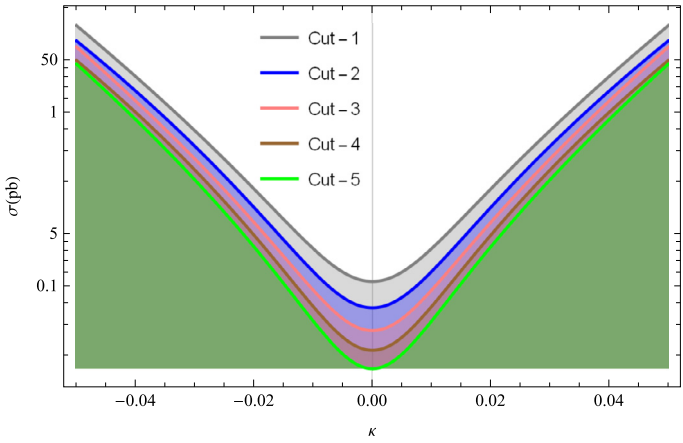

Fig. 8. The total cross sections of the process $\gamma\gamma \to \tau\bar{\tau}\gamma$ with $\sqrt{s} = 500$ GeV beam as a function of the anomalous κ couplings at five different kinematic cuts.

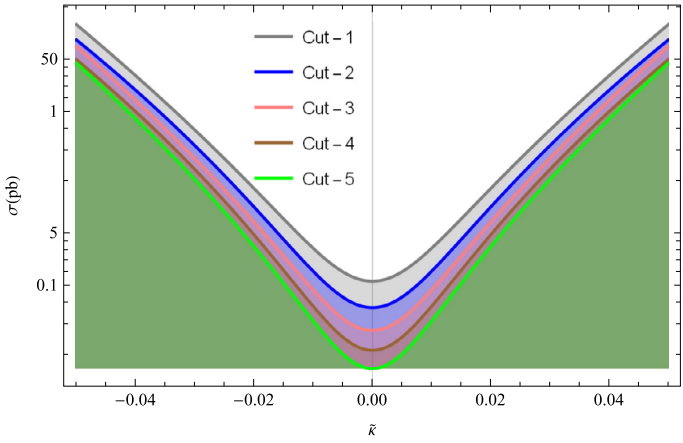

Fig. 9. Same as in Fig. 8, but for the anomalous $\tilde{\kappa}$ couplings.

$$\chi^2 = \left(\frac{\sigma_{SM} - \sigma_{NP}}{\sigma_{SM}\delta}\right)^2, \tag{30}$$

$$\delta = \sqrt{\delta_{stat}^2 + \delta_{sys}^2}, \tag{31}$$

$$N_{SM} = L_{int} \times BR \times \sigma_{SM}, \tag{32}$$

$$\delta_{stat} = \frac{1}{\sqrt{N_{SM}}} \tag{33}$$

where BR, N_{SM} represent branching ratio and number of events. L_{int} shows the integrated luminosity of the ILC. δ_{stat} and δ_{sys} are statistical and systematic uncertainties, respectively. Here, σ_{SM} is the cross section in the SM and σ_{NP} is the cross section containing both the SM and new physics contributions. The tau lepton is the only lepton that has the mass necessary to disintegrate, most of the time in hadrons. In 17.8% of the time, the tau lepton decays into an electron and into two neutrinos; in another 17.4% of the time, it decays in a muon and in

Table 2
Total and SM cross section values and the ratios of total cross section to SM cross section on the anomalous κ and $\tilde{\kappa}$ couplings for three different center-of-mass energies and five different cuts. Here, we assume that the anomalous κ and $\tilde{\kappa}$ couplings are equal to 0.03.

			κ		$\tilde{\kappa}$	
Center-of-mass energy	Cuts	SM cross sections (pb)	Total cross sections (pb)	Ratio	Total cross sections (pb)	Ratio
$\sqrt{s} = 250$ GeV	Cut-1	0.574	2.076	3.617	1.982	3.453
	Cut-2	0.342	1.437	4.202	1.360	3.977
	Cut-3	0.219	1.046	4.776	0.999	4.562
	Cut-4	0.147	0.794	5.401	0.754	5.129
	Cut-5	0.099	0.608	6.141	0.579	5.848
$\sqrt{s} = 350$ GeV	Cut-1	0.605	2.951	4.878	2.825	4.669
	Cut-2	0.395	2.227	5.638	2.134	5.403
	Cut-3	0.275	1.767	6.425	1.691	6.149
	Cut-4	0.199	1.445	7.261	1.379	6.930
	Cut-5	0.147	1.201	8.170	1.150	7.823
$\sqrt{s} = 500$ GeV	Cut-1	0.536	4.107	7.662	3.955	7.379
	Cut-2	0.376	3.334	8.867	3.218	8.559
	Cut-3	0.279	2.820	10.107	2.719	9.746
	Cut-4	0.215	2.447	11.381	2.350	10.930
	Cut-5	0.168	2.145	12.768	2.064	12.286

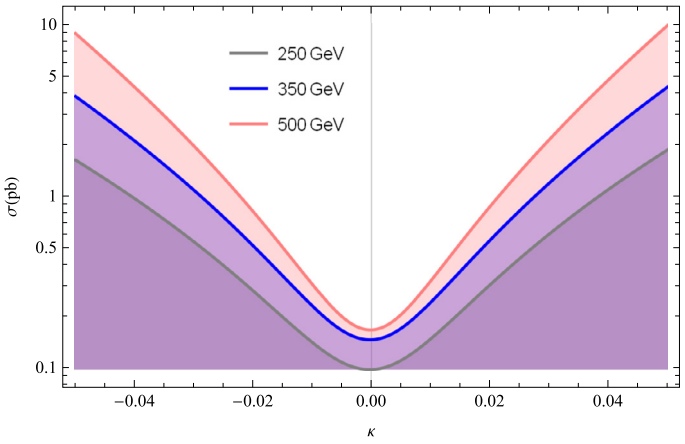

Fig. 10. The total cross sections of the process $\gamma\gamma \to \tau\bar{\tau}\gamma$ depending on the anomalous κ coupling at $\sqrt{s} = 250, 350$ and 500 GeV at the ILC.

two neutrinos. In the remaining 64.8% of the occasions, it decays in the form of hadrons and a neutrino. Here, we take into account pure leptonic and semileptonic decays for tau leptons in the final state. Thus, we assume that in pure leptonic decays BR = 0.123 and in semileptonic decays

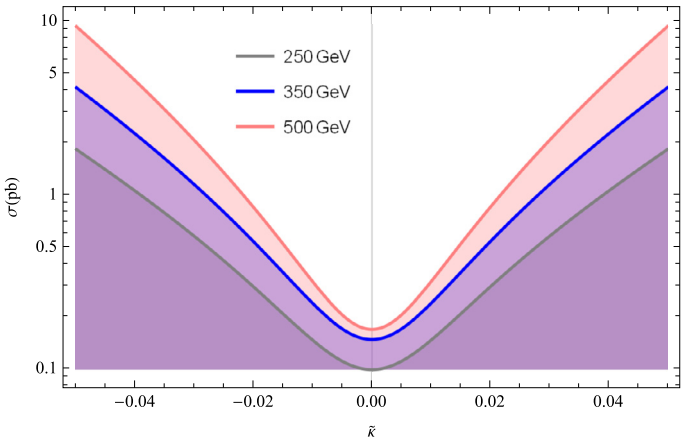

Fig. 11. Same as in Fig. 10, but for the anomalous $\tilde{\kappa}$ coupling.

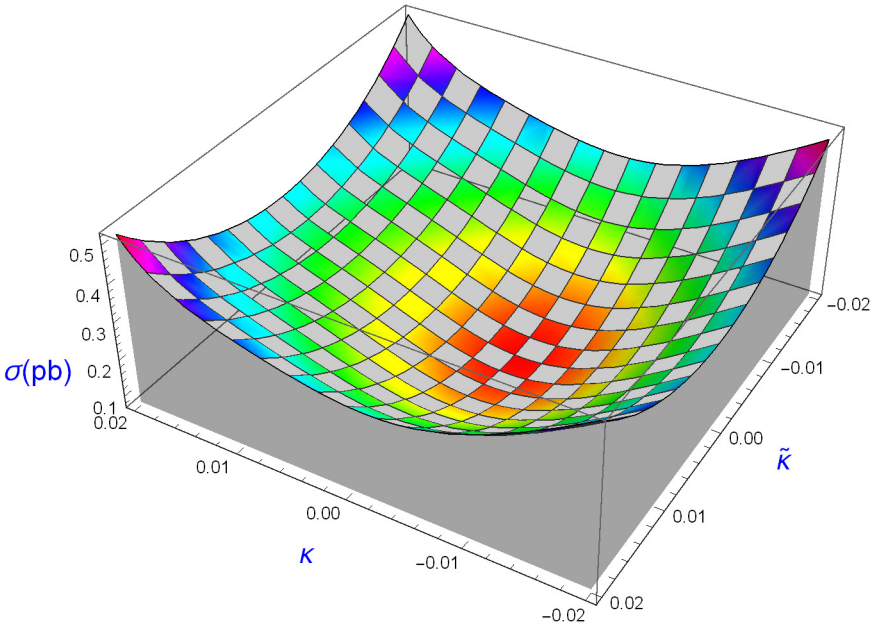

Fig. 12. The total cross sections of the process $\gamma\gamma \to \tau\bar{\tau}\gamma$ depending on the anomalous κ and $\tilde{\kappa}$ couplings at $\sqrt{s} = 250$ GeV at the ILC.

BR = 0.46. Also, we consider each decay channel independently of each other while obtaining the limits on the anomalous couplings. In this study, we do not consider the hadronic decay channel because the systematic uncertainty in this decay channel is considerably greater than in pure leptonic and semileptonic decay channels.

There are systematic uncertainties associated with measuring cross sections involving tau leptons in colliders. Due to these uncertainties, tau identification efficiencies are calculated for the specific process, luminosity, and kinematic parameters. A detailed study is needed to achieve

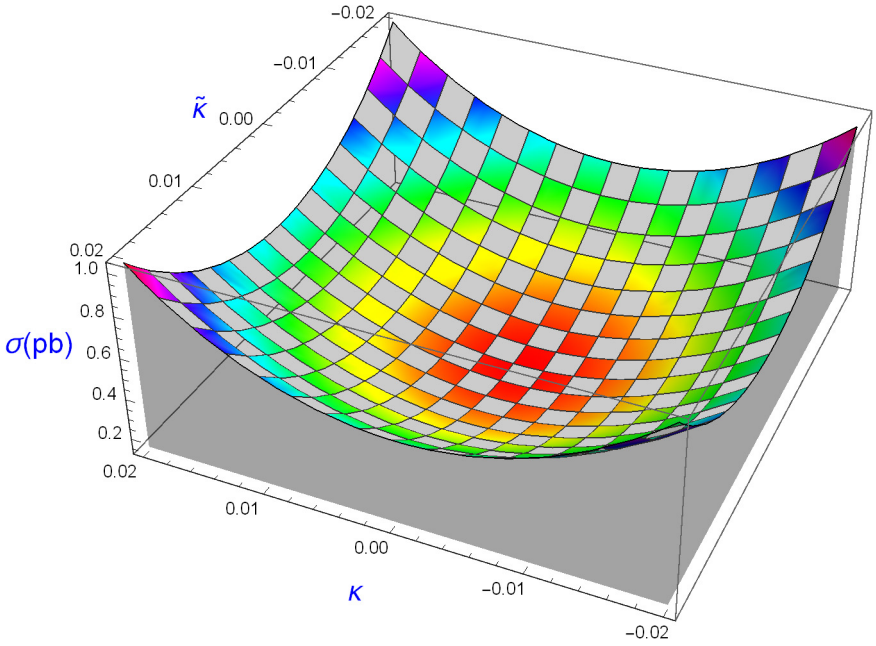

Fig. 13. Same as in Fig. 12, but for $\sqrt{s} = 350$ GeV.

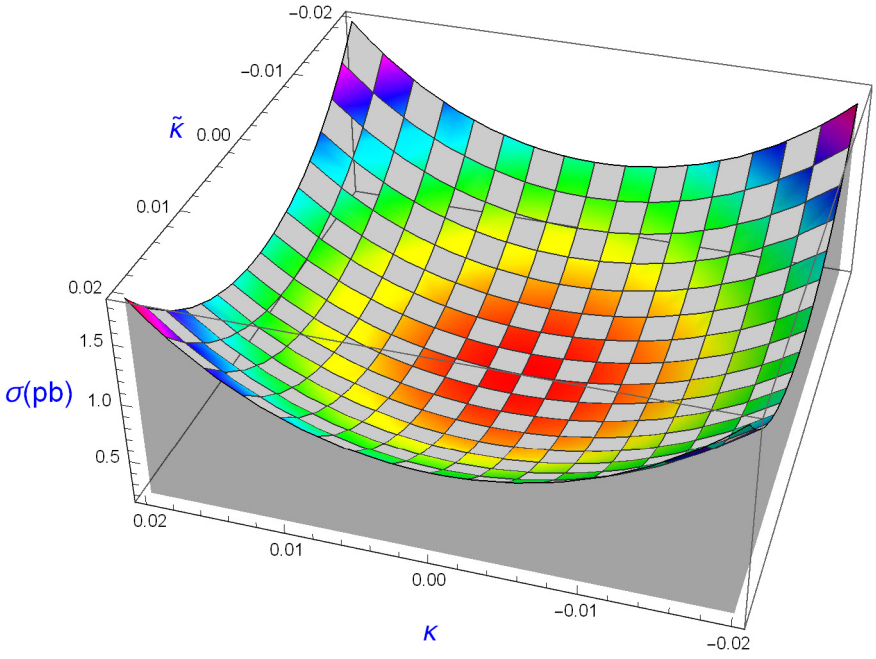

Fig. 14. Same as in Fig. 12, but for $\sqrt{s} = 500$ GeV.

Table 3
For systematic errors of 0, 5% and 10%, the limits on the anomalous couplings at $\sqrt{s} = 250$ GeV ILC through pure leptonic decay channel with integrated luminosities of 100, 500, 1000 and 2000 fb^{-1}.

δ_{sys}	Luminosity (fb^{-1})	$\tilde{a}_\tau$	$\lvert\tilde{d}_\tau\rvert$ (e cm)
0%	100	(-0.00375, 0.00319)	1.91×10^{-17}
	500	(-0.00260, 0.00206)	1.28×10^{-17}
	1000	(-0.00224, 0.00169)	1.08×10^{-17}
	2000	(-0.00193, 0.00139)	9.08×10^{-18}
5%	100	(-0.00520, 0.00462)	2.72×10^{-17}
	500	(-0.00493, 0.00436)	2.57×10^{-17}
	1000	(-0.00490, 0.00433)	2.55×10^{-17}
	2000	(-0.00488, 0.00431)	2.54×10^{-17}
10%	100	(-0.00689, 0.00628)	3.64×10^{-17}
	500	(-0.00678, 0.00618)	3.59×10^{-17}
	1000	(-0.00677, 0.00617)	3.58×10^{-17}
	2000	(-0.00676, 0.00616)	3.58×10^{-17}

a realistic efficiency of a particular process. The systematic uncertainty is not exactly found in any ILC report for the process we are examining. However, there are many studies to probe the anomalous electromagnetic dipole moments of the tau lepton with systematic errors. The systematic uncertainty given at the LEP while investigating the electric and magnetic dipole moments of the tau lepton through the process $e^-e^+ \to e^-e^+\tau^-\tau^+$ was between 4.3% and 8.9% [18]. Ref. [13] has investigated the tau anomalous magnetic moment with systematic errors of 0.1, 1 and 2% at the prospect of future e^-e^+ colliders, such as the ILC, the CLIC, the FCC-ee and the CEPC. The sensitivity limits on the anomalous moments of the tau lepton via the process $e^-e^+ \to e^-e^+\tau^-\tau^+$ at the CLIC were obtained by assuming up to 10% systematic error [34]. The processes $pp \to pp\tau^-\tau^+$ and $pp \to pp\tau\bar{\nu}_\tau j$ were examined from 2% to 7% with systematic uncertainties at the LHC by Refs. [38,39]. In addition, OPAL Collaboration was obtained the bounds on the anomalous magnetic and electric dipole moments of the tau lepton including the systematic uncertainties due to the selection cuts, the photon detection efficiency, non-τ background, binning effects, Monte Carlo statistics and normalization, and the calibration uncertainty in the photon energy measurement through the process $e^-e^+ \to \tau^-\tau^+\gamma$ [17]. For this reason, we obtain limits on the magnetic and electric dipole moments of the tau lepton by 0, 5, 10% systematic errors.

In Tables 3–8, the limits obtained at 95% confidence level on the anomalous $\tilde{a}_\tau$ and $\tilde{d}_\tau$ dipole moments of the tau lepton via the process $\gamma\gamma \to \tau\bar{\tau}\gamma$ in the case of two decay channels at the ILC with $\delta_{sys} = 0, 5, 10\%$ are represented. The best ILC sensitivity limits on the anomalous $\tilde{a}_\tau$ and $\tilde{d}_\tau$ dipole moments of the tau lepton might reach up to the order of magnitude $\mathcal{O}(10^{-4} - 10^{-3})$ and $\mathcal{O}(10^{-18} - 10^{-17})$, respectively. As can be seen in Table 8, the best limits obtained on $\tilde{a}_\tau$ and $\tilde{d}_\tau$ are $-0.00082 < \tilde{a}_\tau < 0.00050$ and $|\tilde{d}_\tau| < 3.59 \times 10^{-18}$ e cm, respectively. Thus, our best limits on the anomalous $\tilde{a}_\tau$ and $\tilde{d}_\tau$ couplings improve much better than the experimental limits.

We observe that the sensitivity obtained on the $\tilde{d}_\tau$ coupling from $\gamma\gamma$ collisions at the 250 GeV ILC are at the same order with the experimental limits, while the sensitivity on $\tilde{a}_\tau$ is expected

Table 4
Same as in Table 3, but for semileptonic decay channel.

δ_{sys}	Luminosity (fb^{-1})	$\tilde{a}_\tau$	$\lvert\tilde{d}_\tau\rvert$ (e cm)
0%	100	(-0.00277, 0.00223)	1.38×10^{-17}
	500	(-0.00195, 0.00141)	9.22×10^{-18}
	1000	(-0.00169, 0.00115)	7.76×10^{-18}
	2000	(-0.00147, 0.00093)	6.52×10^{-18}
5%	100	(-0.00496, 0.00439)	2.58×10^{-17}
	500	(-0.00488, 0.00431)	2.54×10^{-17}
	1000	(-0.00487, 0.00430)	2.54×10^{-17}
	2000	(-0.00486, 0.00430)	2.53×10^{-17}
10%	100	(-0.00679, 0.00619)	3.59×10^{-17}
	500	(-0.00676, 0.00616)	3.58×10^{-17}
	1000	(-0.00676, 0.00616)	3.58×10^{-17}
	2000	(-0.00676, 0.00616)	3.57×10^{-17}

Table 5
For systematic errors of 0, 5% and 10%, the limits on the anomalous couplings at $\sqrt{s} = 350$ GeV ILC through pure leptonic decay channel with integrated luminosities of 10, 50, 100 and 200 fb^{-1}.

δ_{sys}	Luminosity (fb^{-1})	$\tilde{a}_\tau$	$\lvert\tilde{d}_\tau\rvert$ (e cm)
0%	10	(-0.00516, 0.00469)	2.73×10^{-17}
	50	(-0.00353, 0.00308)	1.83×10^{-17}
	100	(-0.00301, 0.00256)	1.54×10^{-17}
	200	(-0.00256, 0.00212)	1.30×10^{-17}
5%	10	(-0.00564, 0.00517)	3.00×10^{-17}
	50	(-0.00466, 0.00420)	2.46×10^{-17}
	100	(-0.00448, 0.00402)	2.36×10^{-17}
	200	(-0.00438, 0.00392)	2.30×10^{-17}
10%	10	(-0.00661, 0.00612)	3.53×10^{-17}
	50	(-0.00610, 0.00562)	3.25×10^{-17}
	100	(-0.00602, 0.00554)	3.21×10^{-17}
	200	(-0.00598, 0.00551)	3.19×10^{-17}

to improve up to two orders of magnitude with respect to experimental results. Also, for semi leptonic decays and without systematic error, our sensitivities on the anomalous couplings for the process $\gamma\gamma \to \tau\bar{\tau}\gamma$ with $\sqrt{s} = 250$ GeV and $L_{int} = 2000$ fb^{-1} can set more stringent up to 1.5 times better than the best sensitivity derived from $\tau\tau\gamma$ production at the ILC with $\sqrt{s} = 350$ GeV and $L_{int} = 200$ fb^{-1}.

Tables 3–8 show that the limits with increasing the luminosity on the anomalous couplings do not increase proportionately to the luminosity due to the systematic error considered here. The reason of this situation is the systematic error which is much bigger than the statistical error. If the systematic error is improved, we expect better limits on the couplings. For example, our best

Table 6
Same as in Table 5, but for semileptonic decay channel.

δ_{sys}	Luminosity (fb^{-1})	$\tilde{a}_\tau$	$\lvert\tilde{d}_\tau\rvert$ (e cm)
0%	10	(-0.00377, 0.00332)	1.97×10^{-17}
	50	(-0.00260, 0.00216)	1.32×10^{-17}
	100	(-0.00223, 0.00178)	1.11×10^{-17}
	200	(-0.00191, 0.00147)	9.31×10^{-18}
5%	10	(-0.00477, 0.00431)	2.52×10^{-17}
	50	(-0.00439, 0.00393)	2.31×10^{-17}
	100	(-0.00433, 0.00387)	2.28×10^{-17}
	200	(-0.00430, 0.00385)	2.26×10^{-17}
10%	10	(-0.00614, 0.00566)	3.28×10^{-17}
	50	(-0.00599, 0.00551)	3.19×10^{-17}
	100	(-0.00597, 0.00549)	3.18×10^{-17}
	200	(-0.00596, 0.00548)	3.18×10^{-17}

Table 7
For systematic errors of 0, 5% and 10%, the limits on the anomalous couplings at $\sqrt{s} = 500$ GeV ILC through pure leptonic decay channel with integrated luminosities of 100, 1000, 2000 and 4000 fb^{-1}.

δ_{sys}	Luminosity (fb^{-1})	$\tilde{a}_\tau$	$\lvert\tilde{d}_\tau\rvert$ (e cm)
0%	100	(-0.00242, 0.00210)	1.26×10^{-17}
	1000	(-0.00144, 0.00112)	7.08×10^{-18}
	2000	(-0.00124, 0.00092)	5.95×10^{-18}
	4000	(-0.00107, 0.00075)	5.01×10^{-18}
5%	100	(-0.00372, 0.00339)	1.98×10^{-17}
	1000	(-0.00358, 0.00325)	1.90×10^{-17}
	2000	(-0.00357, 0.00324)	1.90×10^{-17}
	4000	(-0.00357, 0.00324)	1.90×10^{-17}
10%	100	(-0.00502, 0.00468)	2.70×10^{-17}
	1000	(-0.00497, 0.00463)	2.67×10^{-17}
	2000	(-0.00497, 0.00463)	2.67×10^{-17}
	4000	(-0.00497, 0.00463)	2.67×10^{-17}

limits on the anomalous couplings for the process $\gamma\gamma \to \tau\bar{\tau}\gamma$ with $\sqrt{s} = 500$ GeV, $L_{int} = 4000$ fb^{-1} and $\delta_{sys} = 0\%$ can be improved up to 4 times for $\tilde{a}_\tau$ and 9 times for $\tilde{d}_\tau$ according to case with $\delta_{sys} = 10\%$.

Finally, the contours for the anomalous couplings for the process $\gamma\gamma \to \tau\bar{\tau}\gamma$ at the ILC for various integrated luminosities and center-of-mass energies are presented in Figs. 15–17. As we can see from these figures, the improvement in the sensitivity on the anomalous couplings is achieved by increasing to higher center-of-mass energies and luminosities.

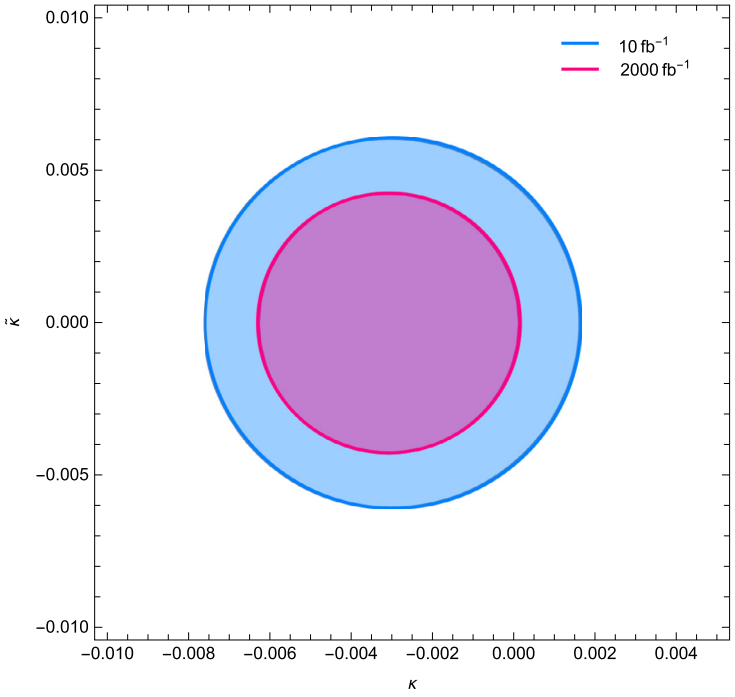

Fig. 15. For semi leptonic decay channel, 95% confidence level contours for anomalous κ and $\tilde{\kappa}$ couplings for the process $\gamma\gamma \to \tau\bar{\tau}\gamma$ with $\sqrt{s} = 250$ GeV and $L_{int} = 10, 2000$ fb^{-1}.

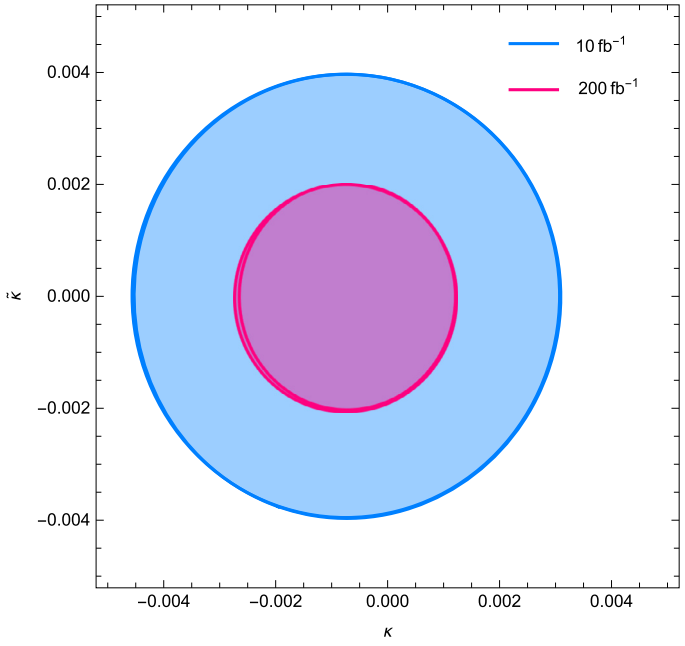

Fig. 16. The same as Fig. 15 but for $\sqrt{s} = 350$ GeV and $L_{int} = 10, 200$ fb^{-1}.

Table 8
Same as in Table 7, but for semileptonic decay channel.

δ_{sys}	Luminosity (fb^{-1})	$\tilde{a}_\tau$	$\lvert\tilde{d}_\tau\rvert$ (e cm)
0%	100	(-0.00179, 0.00147)	9.04×10^{-18}
	1000	(-0.00108, 0.00076)	5.09×10^{-18}
	2000	(-0.00094, 0.00062)	4.28×10^{-18}
	4000	(-0.00082, 0.00050)	3.60×10^{-18}
5%	100	(-0.00361, 0.00328)	1.92×10^{-17}
	1000	(-0.00357, 0.00324)	1.90×10^{-17}
	2000	(-0.00357, 0.00324)	1.89×10^{-17}
	4000	(-0.00357, 0.00324)	1.89×10^{-17}
10%	100	(-0.00498, 0.00464)	2.68×10^{-17}
	1000	(-0.00497, 0.00463)	2.67×10^{-17}
	2000	(-0.00497, 0.00463)	2.67×10^{-17}
	4000	(-0.00496, 0.00463)	2.67×10^{-17}

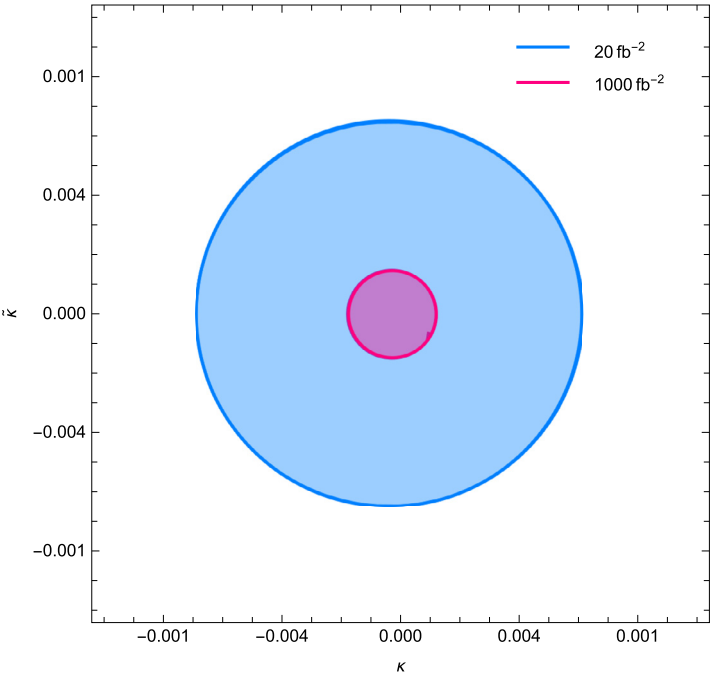

Fig. 17. The same as Fig. 15 but for $\sqrt{s} = 500$ GeV and $L_{int} = 10, 4000$ fb^{-1}.

3. Conclusions

It is of great interest to perform model-independent studies of the magnetic and electric dipole moments of the tau lepton with the processes examined in colliders. The $\tau\bar{\tau}\gamma$ coupling between the tau lepton and the photon needs to be studied precisely. Since non-standard $\tau\bar{\tau}\gamma$ couplings

defined via effective Lagrangian have dimension-six, they have very strong energy dependencies. The cross sections with anomalous couplings increase more quickly with energy than those with SM values. In this case, a possible deviation from the SM cross section of any process involving $\tau\bar{\tau}\gamma$ coupling may be a sign of the existence of the new physics.

The contribution arising the new physics beyond the SM changes the distributions of the kinematic variables of the final state, most notably the photon energy spectrum [17]. Therefore, the p_T distribution of the photon, especially at the region with a large p_T values, is very useful to distinguish signal and background events. In the literature, $e^-e^+ \to \tau\bar{\tau}\gamma$ [17,24] and $Z \to \tau\bar{\tau}\gamma$ [61] processes involving photon in the final state of photon-photon collisions were investigated in order to examine the anomalous magnetic and electric dipole moments of the tau lepton. On the other hand, decay products of the tau leptons are highly collimated because of the QCD jets and this makes them difficult to identify. However, the final state photon identification can facilitate the tau pair identification. Generally, the anomalous parameters tend to increase the cross section for the process $\gamma\gamma \to \tau\tau\gamma$, especially for photons with high energy which are well isolated from the decay products of the taus [24]. Furthermore, the single-photon in the final state has the advantage of being identified with high efficiency and purity. For this reason, we have investigated on the phenomenological aspects of the anomalous $\tau\bar{\tau}\gamma$ couplings with the process $\gamma\gamma \to \tau\bar{\tau}\gamma$ at the ILC.

The total cross section and the limit analysis are analyzed in regard to the anomalous $\tilde{a}_\tau$ and $\tilde{d}_\tau$ dipole moments which cause the possible deviations from the SM. Here, a cutflow is created according to cuts set to achieve optimized limits. The ratio to SM cross section of total cross section including the anomalous $\tilde{a}_\tau$ and $\tilde{d}_\tau$ parameters has determined and the contributions of the kinematic cuts to the signal have examined. Also, for the anomalous $\tilde{a}_\tau$ and $\tilde{d}_\tau$ parameters, the limits at 95% confidence level by using χ^2 test are obtained. We find that the ILC with $\sqrt{s} = 500$ GeV and 4000 fb^{-1} gives the best limits on all the anomalous coupling parameters.

The process $\gamma\gamma \to \tau\bar{\tau}\gamma$ has some advantages. The anomalous $\tau\bar{\tau}\gamma$ couplings can be analyzed via the process $e^-e^+ \to \tau\bar{\tau}\gamma$ at linear colliders. This process receives contributions from both the anomalous $\tau\bar{\tau}\gamma$ and $\tau\bar{\tau}Z$ couplings. Nevertheless, the process $\gamma\gamma \to \tau\bar{\tau}\gamma$ isolates the $\tau\bar{\tau}\gamma$ coupling, and thus $\tau\bar{\tau}\gamma$ and $\tau\bar{\tau}Z$ couplings may be investigated separately. Moreover, the single photon in the final state has the advantage of being identifiable with high efficiency and purity. For this reason, the selection criteria used for the analysis enables examining for events with single-photon characteristics. Finally, $\gamma\gamma$ collisions in lepton colliders may be effective at efficient τ identification due to clean final state when compared to hadron colliders.

Consequently, we emphasize that the sensitivities obtained on the anomalous $\tilde{a}_\tau$ and $\tilde{d}_\tau$ couplings in our work are better than the sensitivity of current experimental limits. $\gamma\gamma$ collisions at the ILC to investigate the anomalous $\tilde{a}_\tau$ and $\tilde{d}_\tau$ couplings via the process $\gamma\gamma \to \tau\bar{\tau}\gamma$ are quite suitable for investigating the anomalous $\tilde{a}_\tau$ and $\tilde{d}_\tau$ dipole moments of the τ lepton.

CRediT authorship contribution statement

M. Köksal: Conceptualization, Investigation, Methodology, Writing – original draft, Writing – review & editing.

Declaration of competing interest

The authors declare that they have no known competing financial interests or personal relationships that could have appeared to influence the work reported in this paper.

References

[1] T. Aoyama, T. Kinoshita, M. Nio, Phys. Rev. D 97 (2018) 036001.
[2] B. Abi, et al., Muon g 2 Collaboration, Phys. Rev. Lett. 126 (2021) 141801.
[3] T. Aoyama, et al., Phys. Rep. 887 (2020) 1–166.
[4] G.W. Bennett, et al., Muon g 2 Collaboration, Phys. Rev. D 73 (2006) 072003.
[5] R.H. Parker, et al., Science 360 (6385) (2018) 191–195.
[6] W. Altmannshofer, S.A. Gadam, S. Gori, N. Hamer, arXiv:2104.08293.
[7] W. Buchmuller, D. Wyler, Nucl. Phys. B 268 (1986) 621–653.
[8] T. Huang, Z.-H. Lin, X. Zhang, Phys. Rev. D 58 (1998) 073007.
[9] M. Fael, Electromagnetic dipole moments of fermions, PhD. Thesis, 2014.
[10] S. Atag, A.A. Billur, J. High Energy Phys. 11 (2010) 060.
[11] X. Chen, Y. Wu, J. High Energy Phys. 10 (2019) 089.
[12] M. Dyndal, M. Klusek-Gawenda, M. Schott, A. Szczurek, Phys. Lett. B 809 (2020) 135682.
[13] H.M. Tran, Y. Kurihara, Eur. Phys. J. C 81 (2) (2021) 108.
[14] S. Atag, E. Gurkanli, J. High Energy Phys. 1606 (2016) 118.
[15] B. Grzadkowski, M. Iskrzynski, M. Misiak, J. Rosiek, J. High Energy Phys. 10 (2010) 085.
[16] M. Acciarri, et al., L3 Collaboration, Phys. Lett. B 434 (1998) 169.
[17] K. Ackerstaff, et al., OPAL Collaboration, Phys. Lett. B 431 (1998) 188.
[18] J. Abdallah, et al., DELPHI Collaboration, Eur. Phys. J. C 35 (2004) 159.
[19] J.H. Christenson, J.W. Cronin, V.L. Fitch, R. Turlay, Phys. Rev. Lett. 13 (1964) 138.
[20] M. Kobayashi, T. Maskawa, Prog. Theor. Phys. 49 (1973) 652.
[21] F. Hoogeveen, Nucl. Phys. B 341 (1990) 322.
[22] J.P. Ma, A. Brandenburg, Z. Phys. C 56 (1992) 97.
[23] S.M. Barr, Phys. Rev. D 34 (1986) 1567.
[24] J. Ellis, S. Ferrara, D.V. Nanopulos, Phys. Lett. B 114 (1982) 231.
[25] A. Gutierrez-Rodriguez, M.A. Hernandez-Ruiz, L.N. Luis-Noriega, Mod. Phys. Lett. A 19 (2004) 2227.
[26] Y. Yamaguchi, N. Yamanaka, Phys. Rev. D 103 (2021) 013001.
[27] Y. Yamaguchi, N. Yamanaka, Phys. Rev. Lett. 125 (2020) 241802.
[28] N. Yamanaka, T. Sato, T. Kubato, J. High Energy Phys. 12 (2014) 110.
[29] N. Yamanaka, Phys. Rev. D 87 (2013) 011701.
[30] K. Inami, et al., BELLE Collaboration, Phys. Lett. B 551 (2003) 16.
[31] L. Beresford, J. Liu, Phys. Rev. D 102 (2020) 113008.
[32] M. Köksal, A.A. Billur, A. Gutierrez-Rodriguez, M.A. Hernandez-Ruiz, Int. J. Mod. Phys. A 34 (15) (2019) 1950076.
[33] M. Köksal, J. Phys. G 46 (2019) 065003.
[34] A.A. Billur, M. Köksal, Phys. Rev. D 89 (2014) 037301.
[35] Y. Ozguven, S.C. Inan, A.A. Billur, M.K. Bahar, M. Köksal, Nucl. Phys. B 923 (2017) 475.
[36] M. Köksal, A.A. Billur, A. Gutierrez-Rodriguez, M.A. Hernandez-Ruiz, Phys. Rev. D 98 (2018) 015017.
[37] J.A. Grifols, A. Mendez, Phys. Lett. B 255 (1991) 611;
J.A. Grifols, A. Mendez, Erratum, Phys. Lett. B 259 (1991) 512.
[38] S. Atag, A.A. Billur, J. High Energy Phys. 1011 (2010) 060.
[39] M. Köksal, S.C. Inan, A.A. Billur, M.K. Bahar, Y. Ozguven, Phys. Lett. B 783 (2018) 375–380.
[40] M.A. Arroyo-Urena, G. Hernandez-Tome, G. Tavares-Velasco, Eur. Phys. J. C 77 (4) (2017) 227.
[41] M.A. Arroyo-Urena, E. Diaz, O. Meza-Aldama, G. Tavares-Velasco, Int. J. Mod. Phys. A 32 (33) (2017) 1750195.
[42] S. Eidelman, D. Epifanov, M. Fael, L. Mercolli, M. Passera, J. High Energy Phys. 1603 (2016) 140.
[43] G.A. Gonzalez-Sprinberg, A. Santamaria, J. Vidal, Nucl. Phys. B 582 (3) (2000).
[44] J. Bernabeu, G. Gonzalez-Sprinberg, J. Papavassiliou, J. Vidal, Nucl. Phys. B 790 (2008) 160.
[45] J. Bernabeu, G.A. Gonzalez-Sprinberg, J. Vidal, J. High Energy Phys. 01 (2009) 062.
[46] M.A. Samuel, G. Li, Int. J. Theor. Phys. 33 (1994) 1471.
[47] R. Escribano, E. Masso, Phys. Lett. B 301 (1993) 419.
[48] R. Escribano, E. Masso, Phys. Lett. B 395 (1997) 369.
[49] A. Pich, Prog. Part. Nucl. Phys. 75 (2014) 41–85.
[50] P. Bambade, et al., arXiv:1903.01629.
[51] C. Adolphsen, et al., arXiv:1306.6353.
[52] V.I. Telnov, Nucl. Part. Phys. Proc. 275 (2016) 224.

[53] H. Terazawa, Rev. Mod. Phys. 45 (4) (1973) 662.
[54] J.M. Yang, Ann. Phys. 316 (2) (2005) 539.
[55] M. Acciarri, et al., L3 Collaboration, Phys. Lett. B 434 (1998) 169.
[56] I.F. Ginzburg, et al., Nucl. Instrum. Methods Phys. Res. 219 (1984) 5.
[57] I. Sahin, J. Phys. G 36 (2009) 075007.
[58] S. Fichet, A. Tonero, P. Rebello Teles, Phys. Rev. D 96 (2017) 036003.
[59] I. Galon, A. Rajaraman, R. Riley, Tim M.P. Tait, J. High Energy Phys. 1612 (2016) 111.
[60] J.N. Howard, A. Rajaraman, R. Riley, Tim M.P. Tait, LHEP 2 (5) (2019).
[61] J.A. Grifols, A. Mendez, Phys. Lett. B 255 (1991) 611;
J.A. Grifols, A. Mendez, Phys. Lett. B 259 (1991), 512(E).